**Advanced Steel Construction** – Vol. 19 No. 1 (2023) 77–85
**DOI:**10.18057/IJASC.2023.19.1.10
(**Special Issue:** *10th International Conference on Advances in Steel Structures, ICASS'2020, Chengdu, China*)


# SEISMIC RESILIENCE ASSESSMENT OF A SINGLE-LAYER RETICULATED DOME DURING CONSTRUCTION

Tian-Long Zhang and Jun-Yan Zhao *

*School of Civil Engineering and Architecture, Hainan University, Haikou, China*
** (Corresponding author: E-mail: jzhaojunyan@hainanu.edu.cn)*

**ABSTRACT**

The seismic bearing capacity of an incomplete single-layer reticulated dome during construction is significantly lower than that of a complete dome. To assess the seismic resilience of incomplete single-layer reticulated domes and find the most unfavorable construction stage, a new curve of recovery functionality and a new methodology of seismic resilience during construction were established in this study. Under the combined action of the bending moment and axial force, the damage state criterion of circular steel pipes was improved through hysteresis simulation analysis. Based on the elastoplastic time-history analysis of different construction models, the damage state levels of all structural members were employed to estimate the functionality loss after an earthquake event. The repair path and the repair time of damaged steel pipes were defined, and the structural recovery functionality was computed to assess the seismic resilience. The proposed methodology in this paper was demonstrated using a 40-meter span of the Kiewitt-8 dome with six circular grids considering both the construction process and seismic hazards. The results indicate that seismic resilience is related to the incomplete structural form of the dome during construction. The repair time will be the longest and the seismic resilience will be the lowest if the incomplete dome suffers an earthquake during the construction period when installing the fourth circular grid from outside to inside.

**ARTICLE HISTORY**

Received: 20 July 2022
Revised: 22 August 2022
Accepted: 10 January 2023

**KEYWORDS**

Single-layer reticulated dome;
Seismic resilience;
Construction model;
Damage state criterion



## 1. Introduction

Due to their light weight, thin thickness, reliable force, and beautiful shape, single-layer reticulated domes are widely used in large span buildings such as airports, stadiums and exhibition halls. Although this type of structure has the mechanical properties of a bar system and a thin shell structure, the existing earthquake hazard shows that members of a dome may experience damage, buckling and fracture to reduce the bearing capacity, threatening lives and the security of property. The dynamic responses and damage modes of complete single-layer reticulated domes under earthquakes have been researched deeply, laying foundations for performance-based seismic design methods of this spatial structure. Fan F. *et al.* [1] defined two types of failure modes of single-layer reticulated domes under a strong earthquake, including dynamic instability and plastic collapse. Zhi X.D. *et al.* [2] proposed different seismic performance levels based on the quantitative damage degree and established a criterion for the dynamic strength failure of single-layer reticulated domes. Nie G.B. *et al.* [3] analyzed the vulnerability curves of single-layer reticulated domes with the IDA method and suggested different overall damage indications. However, the seismic analysis of incomplete domes under construction has rarely been studied.

When a reticulated dome is under construction, the incomplete structural form is constantly changing, and therefore, the internal forces and boundary constraint conditions of the incomplete structure are quite different from those of the complete structure. Many scholars have simulated and analyzed the mechanical performance of spatial reticulated domes during the whole construction process. Liu X.W. *et al.* [4] combined a birth-death finite element technology and a step-by-step model simulation method to conduct a mechanical analysis of steel structures in construction. Tian L.M. *et al.* [5] analyzed the internal force and deformation of a complicated stadium during the construction process by using the finite element method for a large-span structure. Li Y.Y. *et al.* [6] used the finite element software Midas/Gen to simulate construction schemes for a long-span steel roof and studied the effect of different temporary supports under construction. However, the bearing capacity of a structure under construction has not yet been formed, so in this process, the incomplete dome may easily collapse under a strong earthquake, which will seriously affect construction safety, quality and cost. Previous research on the structural construction process has not considered the effect of earthquakes, and few studies have been performed on the seismic response of spatial structures during the construction period.

Seismic resilience refers to the ability to maintain and restore the original function of a structure after earthquake excitation. In the earliest research, Bruneau *et al.* [7] pointed out that seismic resilience can be evaluated from four aspects: robustness, redundancy, rapidity and resourcefulness. In recent years, the study of seismic resilience has mainly been focused on medical systems, water supply systems, bridge engineering and so on. Vásquez *et al.* [8] studied the response and resilience of the healthcare network in Iquique after the Pisagua earthquake in 2014. Favier *et al.* [9] investigated the effect of the Illapel earthquake on local hospitals in 2015. Domaneschi *et al.* [10] studied the immediate seismic resilience of a controlled cable-stayed bridge. Biondini *et al.* [11] studied the life-cycle resilience of deteriorating bridge networks under earthquake scenarios. Dong Y. *et al.* [12] proposed a framework for the probabilistic assessment of an interdependent healthcare-bridge network system under seismic hazards. Pang Y.T. *et al.* [13] assessed the life-cycle seismic resilience of highway bridges with fiber reinforced concrete piers in a corrosive environment by using the improved Cloud Analysis. There are some international standards for seismic resilience assessment of buildings, namely, FEMA-P58 [14], REDi Rating System [15], and USRC Building Rating System [16]. The Chinese standard, GB/T 38591-2020 "Standard for seismic resilience assessment of buildings" [17], was released in 2020. Lu X. [18] proposed a new quantification method of seismic resilience by FEMA-P58 and applied it to evaluate the seismic resilience of typical reinforced concrete frame core pipe tall buildings. Fang D.P. *et al.* [19] assessed the seismic resilience, including the building repair costs, repair time and casualties, in a typical community based on the Chinese standard, GB/T 38591-2020. Clearly, the application of building resilience evaluation standards is gradually becoming mature, and various researchers have carried out partial studies on the seismic resilience evaluation of different structures. However, there has been little research on the seismic resilience assessment of single-layer reticulated domes, especially incomplete domes during construction.

Based on the existing standard for seismic resilience assessment of buildings in China, the process of seismic resilience assessment of a single-layer spherical reticulated dome during construction was developed in this study, and two damage state criterion curves of steel pipe members, with bending moments or axial forces as the main damage, were improved. By taking a 40-meter span of a single-layer spherical reticulated dome as a case study, the seismic resilience in the whole construction process is evaluated.

## 2. Seismic resilience assessment process during construction

Proposed by Bruneau et al. [7], the curve of building recovery functionality *Q(t)* after an earthquake with time history is presented, as shown in Fig. 1(a). When a building system suffers earthquake action at time $t_0$, the building functionality is reduced from 100% to a certain percentage in this figure. Then, the system functionality is later recovered to 100% by a repair path with repair time $T_{RE}$. Bruneau pointed out that the value of seismic resilience is related to the repair time and the recovery functionality curve *Q(t)*. However, this curve is widely used in whole structural and nonstructural members during building operation without considering the change in functionality during construction. The structure of a single-layer reticulated dome during construction is incomplete, leading to the seismic bearing capacity of the incomplete structure

being much lower than that of the complete dome. In addition, the seismic bearing capacity of incomplete structures varies greatly at different times during construction. In this paper, seismic resilience curves during construction are put forward in Fig. 1(b). The structural functionality *Q(t)* monotonically increases from the beginning to the end of the construction. When the incomplete dome suffers an earthquake at time $t_0$ during construction, the functionality will decrease to some degree as well, but it will vary compared to that of a complete dome. The seismically damaged members of incomplete domes must be repaired before construction proceeds. The original construction time $T_C$ will be extended by the repair time $T_{RE}$.

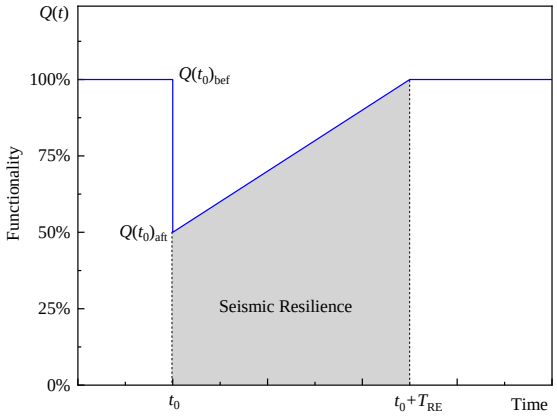


(a) Seismic resilience during operation

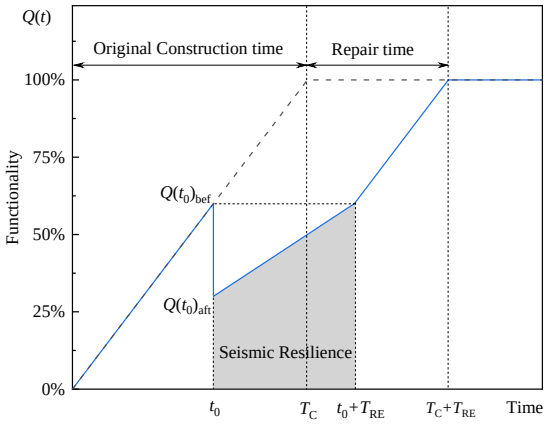


(b) Seismic resilience during construction

**Fig. 1** Curve of recovery functionality and seismic resilience

The seismic resilience assessment of a single-layer reticulated dome during construction should be based on the construction scheme, elastoplastic time-history analysis and damage state criterions of structural and nonstructural members based on the Chinese standard, GB/T 38591-2020. The incomplete structure has not been equipped with nonstructural members, so the damage states of nonstructural members are ignored during construction. Circular steel pipes, welded hollow spherical joints and temporary supports are usually used in single-layer reticulated domes during construction, as shown in Fig. 2, which leads to structural members bearing both large axial forces and bending moments at the bar ends, so circular steel pipes in the dome under earthquakes may have two modes of failure: bending failure modes and axial failure modes. As a result, two damage state criteria of structural members were determined in this study. The whole assessment process of the seismic resilience of a single-layer reticulated dome during construction is shown in Fig. 3 and is described in the following steps.

Step 1: The rational construction scheme of a single-layer reticulated dome must be defined first, especially the construction sequences of different structural members. Then, finite element models in different construction periods should be established, including incomplete structural members and temporary construction support systems.

Step 2: Based on different earthquake hazards, elastoplastic time-history analysis should be carried out using the selected ground motions and the IDA method.

Step 3: Combined with hysteresis experiments or numerical simulations of circular steel pipes, two damage state criteria of structural members considering two failure modes should be determined, including the bending failure mode and axial failure mode.

Step 4: According to the damage criterion, the damage status of all structural members is estimated in different construction models under predetermined earthquake hazards.

Step 5: The repair cost and the repair time of different construction models should be calculated considering the reasonable repair process.

Step 6: The reduced structural functionality should be defined to assess the seismic resilience of a single-layer reticulated dome during construction.

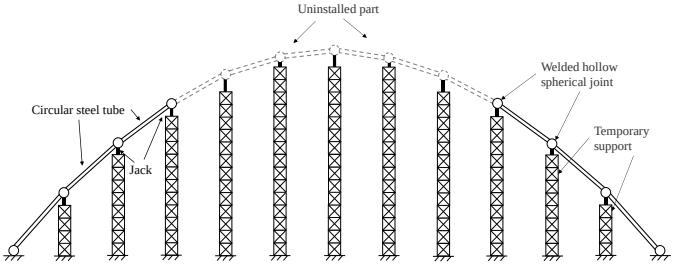


**Fig. 2** The model of a single-layer reticulated dome during construction

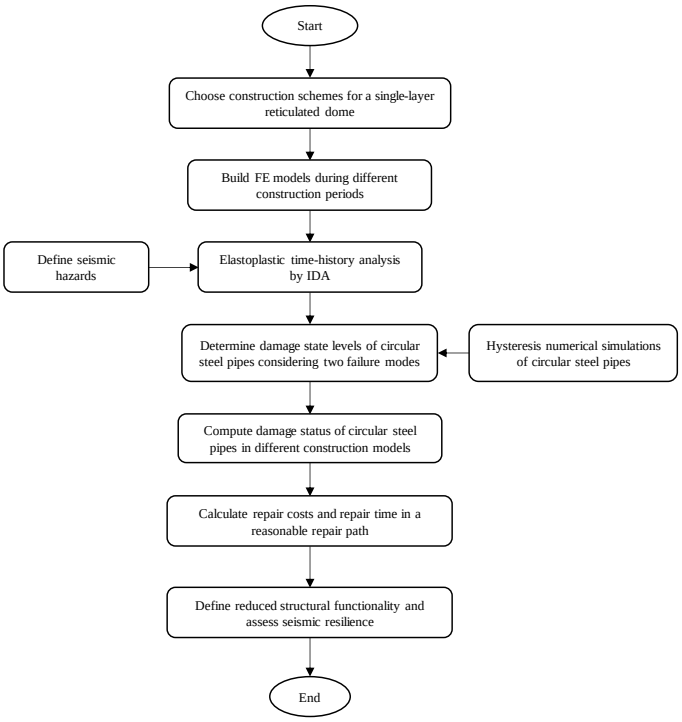


**Fig. 3** The methodology for seismic resilience assessment during construction

## 3. Damage criterion of circular steel pipes

The Chinese standard, GB/T 38591-2020, suggests the damage state criterion in the moment-angle (*M-θ*) curve of steel frame members and force-displacement (*N-Δ*) curve of steel support members with an H-section and rectangular pipes, but the members of a single-layer reticulated dome adopt a circular steel pipe with a large axial force and bending moment at both ends; these characteristics are not specified in this standard. The bending failure of the member may occur when the bending moment is larger, but when the axial force becomes larger, the bar may yield by tension or buckle by compression. As a result, the mode of bending failure or axial failure must be distinguished by the damage criteria. To obtain the different damage criterion curves of circular steel pipes in a single-layer reticulated dome, hysteresis analysis must be carried out by component tests or numerical simulations. In this paper, two mechanical models are established to study the damage criterion of circular steel

pipes with rigid connection joints under cyclic bending moments or cyclic axial forces by finite element analysis simulation, as shown in Fig. 4. Because the bending stress or axial stress in a circular steel pipe is dominant, two types of mechanical models are taken as the research object by the numerical simulation method. The hysteretic performances of different types of members are analyzed in different loading systems and member parameters, such as component length and sectional dimension.

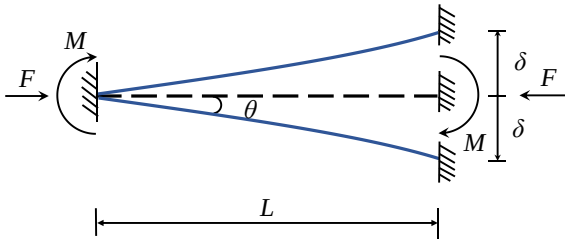


(a) Hysteresis simulation of the bending moment

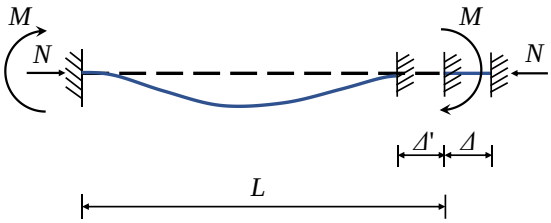


(b) Hysteresis simulation of the axial force

**Fig. 4** Mechanical models of the circular steel pipe

Fig. 4(a) shows the mechanical model of a circular steel pipe with a cyclic bending moment. One end of the bar is consolidated, and the lateral loading system at the other end is controlled by the lateral displacement $\delta$ , while the axial compression force $N$ in the bar remains constant. The lateral displacement adopted the cyclic loading method, and the loading system is shown in Fig. 5(a). A schematic diagram of the loading system is shown in Fig. 5(a), in which the X-axis $n$ represents the number of loading cycles, and the Y-axis represents the ratio of the lateral displacement $\delta$ to the yield displacement $\delta_y$. The yield lateral displacement $\delta_y$ of the circular steel pipe is calculated by Eq. 1:

$$\delta_y = \frac{2\left(f_y - F/A\right)L^2}{3ED} \tag{1}$$

where $\delta_y$ is the lateral yield displacement; $f_y$ is the actual yield stress of steel; $L$ is the length of the bar; $F$ is the constant axial compression force; $E$ is the elastic modulus of steel; and $D$ is the outer diameter of the bar section.

Fig. 4(b) shows the mechanical model of the circular steel pipe with an axial force. One end of the bar is consolidated, and the loading system at the other end is controlled by axial displacement $\Delta$ when the bending moment $M$ is constantly 0.2 times the bending yield bearing capacity. The axial displacement adopts the cyclic loading method, and the loading system is shown in Fig. 5(b), in which abscissa n represents the number of loading cycles and ordinate $\Delta$ represents the cyclic axial displacement. $L$ represents the length of the bar, a positive value indicates tensile displacement, and a negative value indicates compressive displacement. The yield axial displacement $\Delta_y$ of the circular steel pipe is calculated by Eq. 2:

$$\Delta_y = \frac{\left(f_y - M/W\right)L}{E} \tag{2}$$

where $\Delta_y$ is the axial yield displacement; $f_y$ is the actual yield stress of steel; $L$ is the length of the bar; $M$ is the constant bending moment; $E$ is the elastic modulus of steel; and $W$ is the section modulus of the bar.

The aforementioned hysteresis simulation of circular steel pipes should yield the skeleton curves of the $M$-$\theta$ and $N$-$\Delta$ models. These skeleton curves can be the damage state criterion of circular steel pipes in a single-layer reticulated dome, and according to the Chinese standard, GB/T 38591-2020, the damage state of steel structural members is divided into five levels, as shown in Fig. 6. The five levels include Level 0 (Intact), which means no damage occurs; Level 1 (Slight), which means that only minor damage affecting appearance occurs; Level 2 (Moderate), which means moderate damage that can be repaired simply occurs; Level 3 (Extensive), which means general damage that can be repaired to full structural function by conventional methods occurs; and Level 4 (Complete), which means serious damage that affects the bearing capacity or requires component replacement occurs.

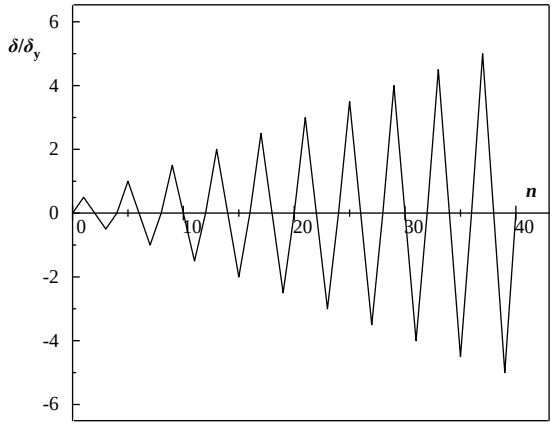


(a) Cyclic lateral displacement

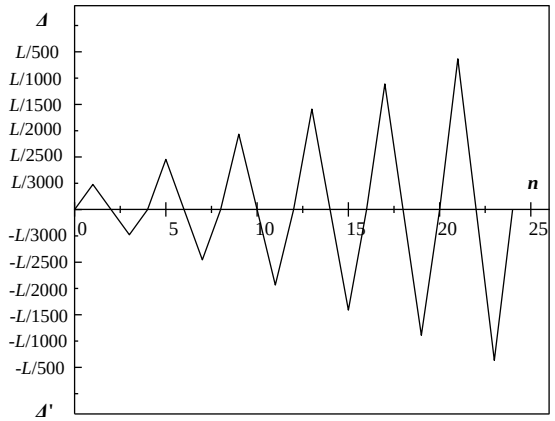


(b) Cyclic axial displacement

**Fig. 5** Hysteresis load curves of the circular steel pipe

As shown in Fig. 6, the $M$-$\theta$ criterion of bending failure and $F$-$\Delta$ criterion of tensile failure or compressive failure are represented by 4 broken line models. $\theta_B$, $\theta_{IO}$, $\theta_{LS}$, $\theta_C$ and $\theta_{CP}$ represent the angle of the component corresponding to nominal yield point B, performance point IO, performance point LS, peak point C and failure point CP, respectively. $\Delta_B$, $\Delta_{IO}$, $\Delta_{LS}$, $\Delta_C$ and $\Delta_{CP}$ represent the tensile displacement of the component corresponding to nominal yield point B, performance point IO, performance point LS, peak point C and failure point CP, respectively. $\Delta'_B$, $\Delta'_{IO}$, $\Delta'_{LS}$, $\Delta'_C$ and $\Delta'_{CP}$ represent the compressive displacement of the component corresponding to nominal yield point B, performance point IO, performance point LS, peak point C and failure point CP, respectively. The damage state level of each member should be determined by the most unfavorable index calculated in the $M$-$\theta$ and $F$-$\Delta$ damage state criteria.

## 4. Calculation of seismic resilience

### *4.1. Calculation of repair time*

To assess the seismic resilience, the repair time must be calculated according to Fig. 1. The repair time of a single-layer reticulated dome are closely related to different grid positions and repair paths of damaged structural members. In this study, the repair path of the damaged dome is from low grids to high grids, namely, from outside grids to inside grids. The repair path of each grid is that the damaged radial members should be repaired at first, and then the damaged annular members and damaged diagonal members are repaired subsequently. According to the repair principle of a reticulated dome after a disaster proposed by Reference [20], the repair methods of structural members in different damage state levels are shown in Table 1.

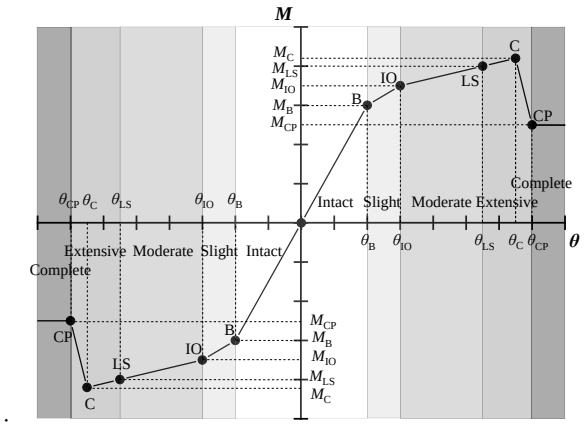


(a) *M*-*θ* curve for bending failure

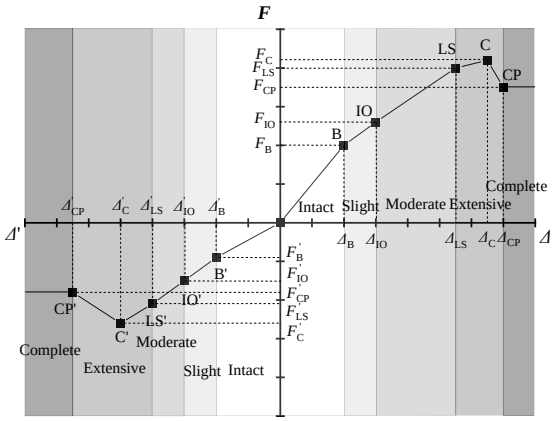


(b) *F*-*Δ* curve for axial failure

**Fig. 6** Damage state criteria of the circular steel pipe

**Table 1**
Repair method of structural members at different damage state levels

| Level 0 (Intact) | Level 1 (Slight) | Level 2 (Moderate) | Level 3 (Extensive) | Level 4 (Complete) |
|---|---|---|---|---|
| Reserve the intact bar | Straighten the bar with special machines | Replace the damaged bar with new one | | |

The total construction repair time of all damaged structural members should meet the requirements to recover structural function. To facilitate calculation, it is not necessary to include the time spent in seismic damage assessment, repair path planning, repair material procurement, construction equipment leasing and other preparatory work before repair. The repair time of different types of structural members under different damage states is calculated by Eq. 3, which is related to the repair time of a single worker to complete the work, the number effect of the damaged structural members and efficiency improvement of member repair.

$$Q_i = \sum_{j=1}^{n} (Q_{(i,j)} \times n_{(i,j)}) \times \zeta_{T(i)} \tag{3}$$

where $Q_i$ is the repair time of type $i$ members (man-days); $Q_{(i,j)}$ is the repair time of type $i$ members under damage state $j$, which was suggested by Reference [20] and Reference [21], as shown in Table 2; $n_{(i,j)}$ is the number of type $i$ members under damage state $j$ (man-days); and $\zeta_{T(i)}$ is the reduction coefficient of the repair time considering the damaged number of type $i$ member, as shown in Table 3.

**Table 2**
Repair time of structural members in different damage state levels

| $i$ | Structural member type | Repair time in different damage state levels $j$ (man-days) | | | | |
|---|---|---|---|---|---|---|
| | | Level 0 (Intact) | Level 1 (Slight) | Level 2 (Moderate) | Level 3 (Extensive) | Level 4 (Complete) |
| 1 | Radial bar | 0 | 2 | 15 | 15 | 15 |
| 2 | Diagonal bar | 0 | 2 | 15 | 15 | 15 |
| 3 | Annular bar | 0 | 2 | 15 | 15 | 15 |

**Table 3**
Reduction coefficient of repair time considering the number of damaged members

| $i$ | Structural member type | Number of damaged members | | |
|---|---|---|---|---|
| | | ≤10 | 11~49 | ≥50 |
| 1 | Radial bar | 1.0 | linear interpolation | 0.8 |
| 2 | Diagonal bar | 1.0 | | 0.8 |
| 3 | Annular bar | 1.0 | | 0.8 |

The total repair time of all damaged structural members is calculated by Eq. 4, which is related to the number of repaired workers and the sum of the repair time for different types of damaged structural members.

$$T_{RE} = \frac{\sum_{i=1}^{3} Q_i}{N} \tag{4}$$

where $T_{RE}$ is the total repair time of the single-layer reticulated dome (man-days), and $N$ is the number of workers repairing damaged structural members.

*4.2. Calculation of structural recovery functionality*

The structural recovery functionality suggested in FEMA-P58 refers to the relationship between the time and the structural recovery functionality before or after an earthquake. Due to the concepts of redundancy and robustness, the structural recovery functionality of the single-layer reticulated dome is related to the number of damaged members and the damage state level of each damaged member. To establish the relationship between the damaged members and the structural recovery functionality, by combining the different repair methods and different damage state levels, it is assumed that the influence coefficient of the damaged member is linearly proportional to its repair time, and the influence coefficient of the member to be replaced is 1.0 in this paper. The overall structural damage index of the single-layer reticulated dome is specified as Eq. 5:

$$\bar{D} = \frac{\sum_{j=0}^{4} D_j \times n_j}{\sum_{j=0}^{4} n_j} \tag{5}$$

where $\bar{D}$ is the overall structural damage index of the dome; $D_j$ is the damage index of each member in damaged state level $j$, with the values shown in Table 4; and $n_j$ is the total number of members in damaged state level $j$.

**Table 4**
Damage index of each damaged structural members

| $i$ | Structural member type | Damage index in different damage state levels $j$ | | | | |
|---|---|---|---|---|---|---|
| | | Level 0 (Intact) | Level 1 (Slight) | Level 2 (Moderate) | Level 3 (Extensive) | Level 4 (Complete) |
| 1 | Radial bar | 0 | 0.1 | 1 | 1 | 1 |
| 2 | Diagonal bar | 0 | 0.1 | 1 | 1 | 1 |
| 3 | Annular bar | 0 | 0.1 | 1 | 1 | 1 |

The structural functionality of the incomplete single-layer reticulated dome during construction is related to the percentage of installed bars so that at time

$t_0$ before the earthquake, the structural functionality $Q(t_0)_{\text{bef}}$ is specified as Eq. 6:

$$Q(t_0)_{\text{bef}} = \frac{n_{\text{install}}}{n_{\text{total}}} \times 100\% \tag{6}$$

where $n_{\text{install}}$ is the number of installed members at time $t_0$ during construction, and $n_{\text{total}}$ is the total number of installed members of the complete single-layer reticulated dome. After the earthquake, the structural functionality of the damaged dome $Q(t_0)_{\text{aft}}$ is specified as Eq. 7:

$$Q(t_0)_{\text{aft}} = Q(t_0)_{\text{bef}}(1-\overline{D}) \tag{7}$$

Because the single-layer reticulated dome in this study only consists of structural members but no nonstructural components during construction, the linear recovery functionality suggested by Reference [18] is adopted as Eq. 8:

$$Q(t,T_{\text{RE}}) = a(\frac{t-t_0}{T_{\text{RE}}}) + b \tag{8}$$

where $t_0$ is the time when the earthquake occurs; $T_{\text{RE}}$ is the repair time of all damaged structural members after the earthquake; and $a$ and $b$ are constant values of 1 and -1, respectively. Based on the recovery functionality during construction and the repair time $T_{\text{RE}}$, the seismic resilience of a single-layer reticulated dome during construction is expressed as Eq. 9, as recommended by Reference [23]:

$$R = \frac{\int_{t_0}^{t_0+T_{\text{RE}}} Q(t,T_{\text{RE}})dt}{T_{\text{RE}}} \tag{9}$$

Eq. 9 shows that the smaller the reduction area of structural functionality is, the larger seismic resilience $R$ is, and the shorter the repair time is, the larger seismic resilience $R$ is.

## 5. Case study

### *5.1. Finite element model*

The presented methodology for the seismic resilience during construction was studied by a typical Kiewitt-8 dome, as shown in Fig. 7. The span of this dome is 40 m, and the rise-to-span ratio is 1/4. The boundary conditions include fixed hinge supports, and the material is Q235 steel, with a yield strength of 235 MPa, a density of 7850 kg/m$^3$ and an elastic modulus of 2.06×10$^5$ MPa. The number of gird circles is 6, and the roof dead load is 1 kN/m$^2$. Different pipe sections of the single-layer reticulated dome and temporary support system during construction are shown in Table 5. The type of temporary support system is a latticed column.

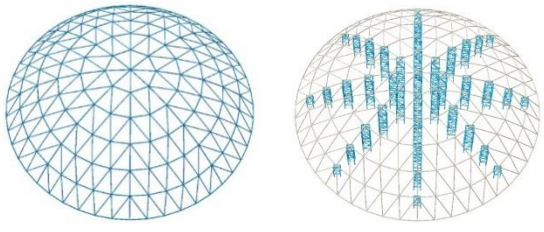

(a) Single-layer reticulated dome (b) Temporary support system

**Fig. 7** Case model

The finite element model was established by ABAQUS software. The element type of the members is B31, and the beam sections are circular pipes. The connection of the structural member of the single-layer reticulated dome is rigid, and the joints of the temporary support members are hinge joints. The connector element was adopted to simulate the interaction between the temporary support and the dome structure. Temporary support only provides vertical compressive force and does not provide tension force when separating during earthquake actions. The constitutive model of the steel material and the mechanical model of the connector element are shown in Fig. 8.

**Table 5**
Pipe section of the single-layer reticulated dome and temporary support system

| Kiewitt-8 dome | Pipe section | Temporary supports | Pipe section |
|---|---|---|---|
| Radial bar | Φ133×4 | Vertical bar | Φ108×8 |
| Annular bar | Φ133×4 | horizontal bar | Φ90×6 |
| Diagonal bar | Φ114×3 | Diagonal bar | Φ90×6 |

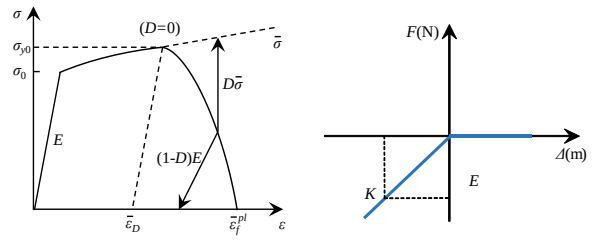


(a) Stress–strain curve of steel (b) Force displacement curve of connector elements

**Fig. 8** Mechanical curves of the FE model

### *5.2. Damage criterion of dome members*

Hysteresis simulations of different circular steel pipes in the dome were carried out under a cyclic bending moment or a cyclic axial force. As a result, two damage failure modes of the circular steel pipe by hysteresis simulation are shown in Fig. 9. Fig. 9 indicates that bending failure under cyclic bending moment leads to the overall instability of the member and that axial failure under cyclic axial force leads to the local buckling of the member.

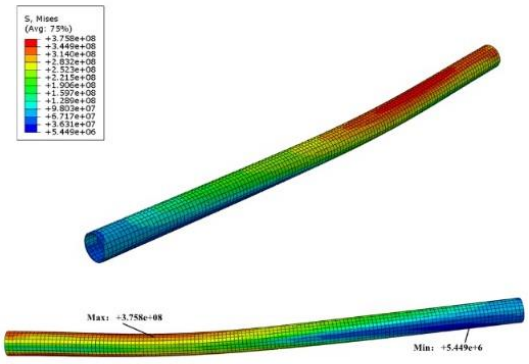


(a) Bending failure under cyclic bending moment

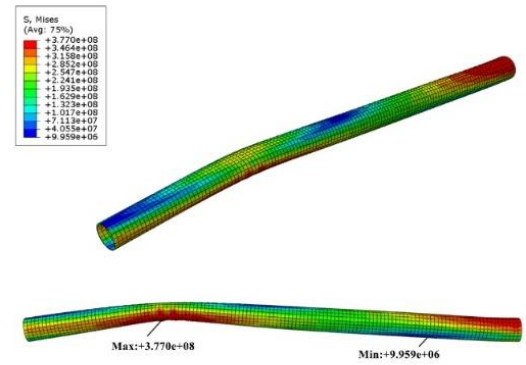


(b) Axial failure under cyclic axial force

**Fig. 9** Two types of failure modes for dome pipes

Hysteresis curves of the radial bar, the diagonal bar and the annular bar in

the dome under two loading systems are shown in Fig. 10. Fig. 10 (a) indicates that the diagonal bar with a larger slenderness ratio has a lower bending moment capacity and easily undergoes bending failure. Fig. 10 (b) indicates that the compressive bearing capacity of the dome member is much lower than its tensile bearing capacity. The skeleton curve was the outsourcing curve by connecting the maximum peak points of each cycle in the hysteresis curve. Fig. 11 shows skeleton curves of the radial bar, the diagonal bar and the annular bar in the dome under two loading systems.

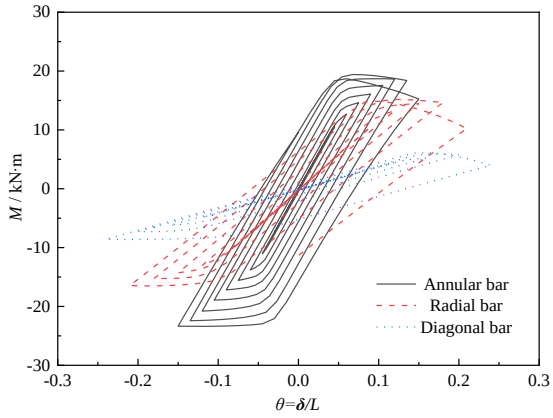


(a) *M-θ* curve under cyclic bending moment

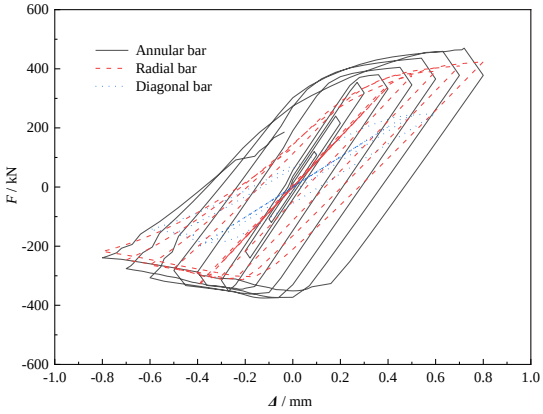


(b) *F-Δ* curve under cyclic axial force

**Fig. 10** Hysteresis curves of the circular steel pipes

From the skeleton curves, the damage criterion of different types of dome members was obtained, as shown in Table 6, Table 7 and Table 8. Compared with the Chinese standard, GB/T 38591-2020 [17], the values of $\theta$ and $\Delta$ at each damaged state level are smaller. This is because steel structural members in a single-layer reticulated dome are both bearded with simultaneous bending moments and axial forces. The combined action of the bending moment and axial force facilitates damage to the structural members so that the index of the damage criterion is reduced, especially the index of axial displacement $\Delta$. Taking the annual bar as an example, the *M-θ* damage criterion and *F-Δ* damage criterion are shown in Fig. 12.

**Table 6**
$\theta$ value of the damage state criterion of steel structural members

| Representative specification | Structural member type | Member section | $\theta_{IO}/\theta_y$ | $\theta_{LS}/\theta y$ | $\theta_u/\theta_y$ |
|---|---|---|---|---|---|
| Chinese Standard: GB/T 38591-2020 | Steel beam | H-section | 1.25 | 4 | 5 |
| | Steel column | H-section | 1.25 | 4 | 5 |
| | Steel column | Rectangular tube | 1.25 | 4 | 5 |
| Recommended in this paper | Radial bar | Circular pipe | 1.1 | 2.5 | 3 |
| | Diagonal bar | | 1.1 | 2.5 | 3 |
| | Annular bar | | 1.1 | 4 | 5 |

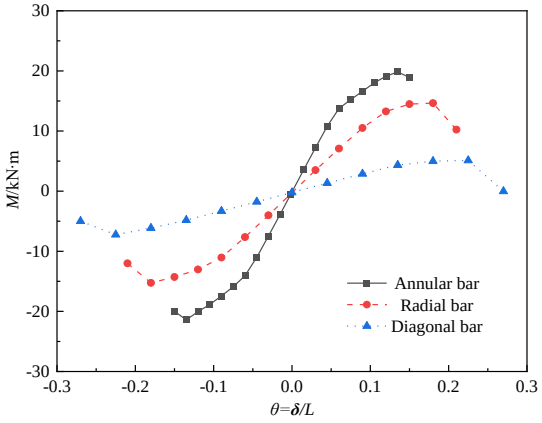


(a) *M-θ* curve under cyclic bending moment

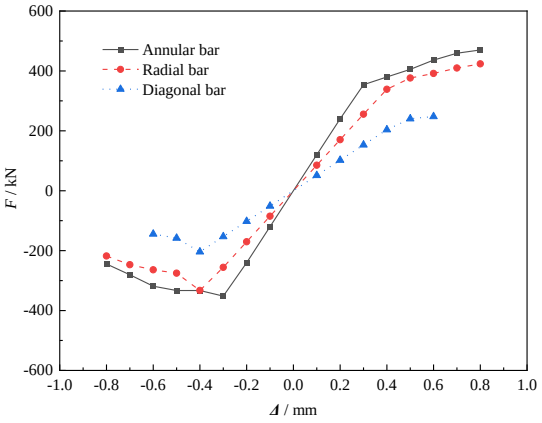


(b) *F-Δ* curve under cyclic axial force

**Fig. 11** Skeleton curves of the circular steel pipes

**Table 7**
$\Delta'$ value of the damage state criterion of compressive structural members

| Representative specification | Structural member type | Member section | $\Delta'_{IO}/\Delta'_y$ | $\Delta'_{LS}/\Delta'_y$ | $\Delta'_u/\Delta'_y$ |
|---|---|---|---|---|---|
| Chinese Standard: GB/T 38591-2020 | Steel Support | H-section | 1.5 | 8 | 9 |
| | | Rectangular tube | 1.5 | 7 | 8 |
| Recommended in this paper | Radial bar | Circular pipe | 1.1 | 1.3 | 1.5 |
| | Diagonal bar | | 1.1 | 1.3 | 1.5 |
| | Annular bar | | 1.1 | 1.5 | 2.0 |

**Table 8**
$\Delta$ value of the damage state criterion of tensile structural members

| Representative specification | Structural member type | Member section | $\Delta_{IO}/\Delta_y$ | $\Delta_{LS}/\Delta_y$ | $\Delta_u/\Delta_y$ |
|---|---|---|---|---|---|
| Chinese Standard: GB/T 38591-2020 | Steel Support | H-section | 1.5 | 8 | 10 |
| | | Rectangular tube | 1.5 | 8 | 10 |
| Recommended in this paper | Radial bar | Circular pipe | 1.3 | 1.8 | 2.5 |
| | Diagonal bar | | 1.3 | 1.8 | 2.5 |
| | Annular bar | | 1.3 | 2.1 | 2.7 |

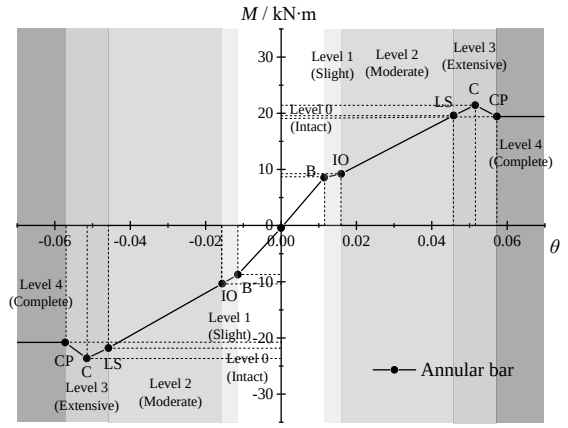


(a) *M-θ* damage state criterion

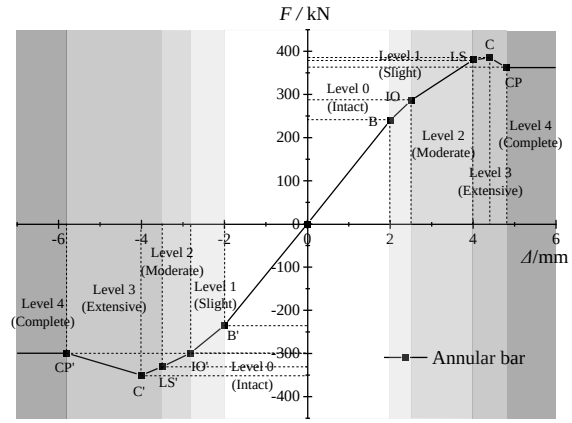


(b) *F-Δ* damage state criterion

**Fig. 12** Damage state criterion of the annual bar

### *5.3. Seismic resilience assessment of the dome during construction*

By dividing the single-layer reticulated dome into six circular grids from outside to inside, scattered assembly technology at high altitude was adopted during construction. As temporary supports, the latticed columns were arranged under each joint at both ends of all dome members. Because the dome structure is symmetrical, the symmetrical construction method was adopted to ensure construction safety. The specific construction steps and temporary support models are shown in Fig. 13. According to Chinese code GB 50011-2016: "Code for Seismic Design of Buildings" [24], seismic hazards are defined as frequent earthquakes, moderate earthquakes and rare earthquakes. Taking the peak ground acceleration (PGA) as the index of ground motion intensity. 3D earthquakes, including the El Centro Earthquake wave, Taft Earthquake wave, Loma Prieta Earthquake wave and Tianjin Earthquake wave, were adopted to conduct an elastoplastic time-history analysis. The PGA of the seismic waves was adjusted to 110 cm/s$^2$, 300 cm/s$^2$ and 510 cm/s$^2$. The PGA ratio in the X, Y and Z directions was 1:0.85:0.65.

The time-history analysis of incomplete dome models under different construction steps was carried out by using ABAQUS. The relative axial displacement and relative rotation angle were calculated by obtaining the coordinates of each member joint. Combined with the proposed *M-θ* damage criterion in Table 6 and the *F-Δ* damage criterion in Table 7, the damage state level and the final failure mode of each member were determined by the higher value of the damage state criteria. The average damage state levels and the average failure modes of all members in different construction models under different rare earthquakes were calculated, as shown in Fig. 14. Fig. 14(a) shows that the percentage of damaged members varies widely at different construction steps, as does the seismic bearing capacity of the incomplete dome during construction. The percentage of damaged members in the model under construction Step 14 is 40.51%, which is the maximum value during construction. That is, when the fourth circular grid is installed in Step 14, this construction model is the most unfavorable with the most damaged members. Fig. 14(b) indicates that there are two failure types of damaged members in the single-layer reticulated dome during construction, and the percentage of member failure modes changes widely at different construction steps. The results also show that the construction model under Step 14 is the most unfavorable model during construction. When the dome is completely built, there are no damaged members under rare earthquakes, so the seismic bearing capacity of the complete single-layer reticulated dome is larger than that of the incomplete dome.

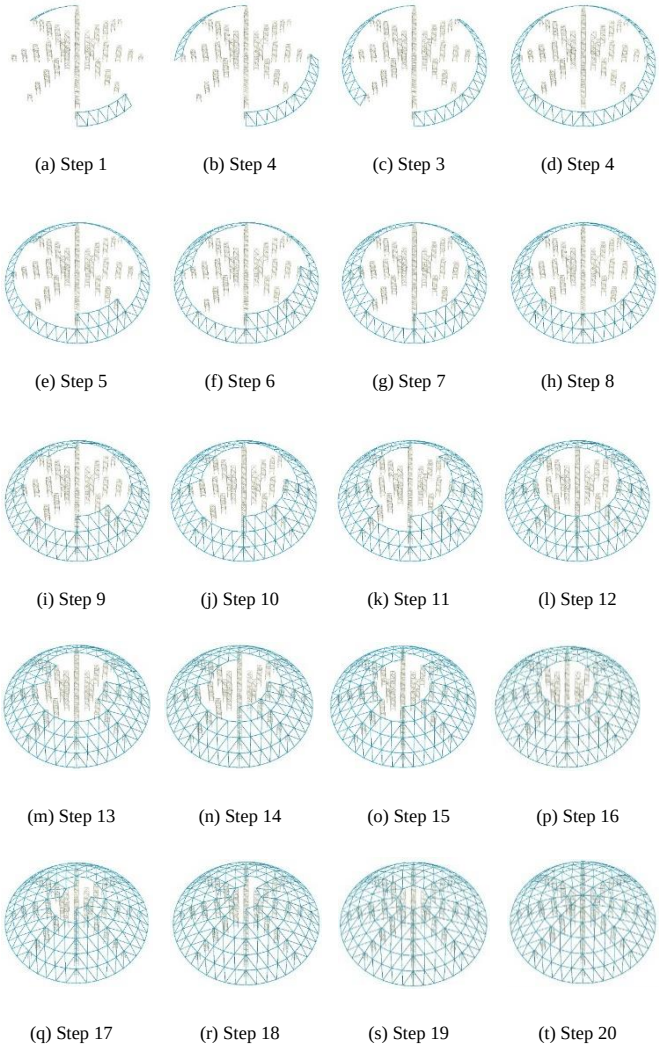

(a) Step 1 (b) Step 4 (c) Step 3 (d) Step 4

(e) Step 5 (f) Step 6 (g) Step 7 (h) Step 8

(i) Step 9 (j) Step 10 (k) Step 11 (l) Step 12

(m) Step 13 (n) Step 14 (o) Step 15 (p) Step 16

(q) Step 17 (r) Step 18 (s) Step 19 (t) Step 20

**Fig. 13** Construction models of a single-layer reticulated dome

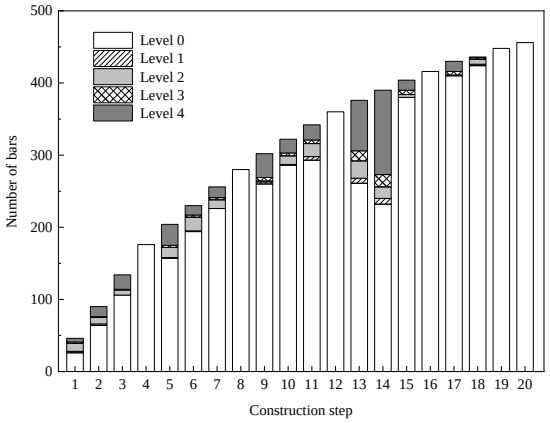


(a) Damage state levels

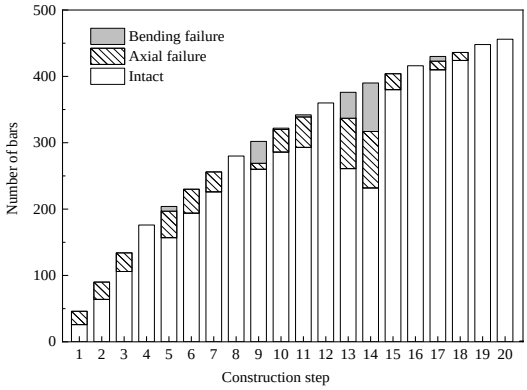


(b) Member failure modes

**Fig. 14** Damaged member results under each construction step

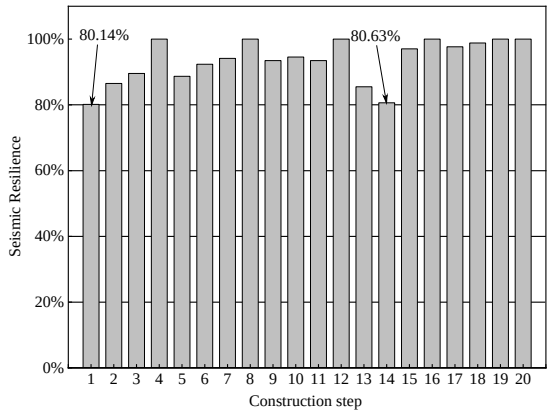


(b) Value of seismic resilience

**Fig. 15** Seismic resilience assessment under construction

Through Eq. 3~Eq. 4, the average repair time ($T_{RE}$) in different construction models under different rare earthquakes was calculated, as shown in Fig. 15(a). Fig. 15(a) shows that the repair time is when the fourth circular grid is installed at Step 14. The average repair time reaches 1814 man-days after a rare earthquake, and 90% of the damaged members need to be replaced. That is, if 26 workers are arranged to repair the damaged members, then the repair time is 70 days, and the total construction period is extended by 70 days. Through Eq. 5~Eq. 9, the average seismic resilience of different construction models under different rare earthquakes was calculated, as shown in Fig. 15(b). Fig. 15(b) suggests that the value of seismic resilience at construction Step 1 is 80.14% and the value of seismic resilience at construction Step 14 is 80.63%, which are the two lowest numbers. This result demonstrates that when the first and fourth circular grids are under construction, the structural functionality decreases the most significantly during these two periods. Special attention should be given to the seismic safety of these two construction periods.

Taking the construction model at step 14 as an example, the average value of seismic resilience ($R$) and recovery functionality curves under different earthquake hazards are shown in Fig. 16. This result illustrates that the average seismic resilience under frequent earthquakes, moderate earthquakes and rare earthquakes is 0.91, 0.85 and 0.81, respectively, and if 26 workers are arranged to repair the damaged members, the repair time under frequent earthquakes, moderate earthquakes and rare earthquakes is 33 days, 51 days and 70 days, respectively. With increasing earthquake intensity, the value of seismic resilience decreases, and the repair time increases. Special measures should be taken to control the seismic safety of the most unfavorable construction periods by seismic resilience assessment.

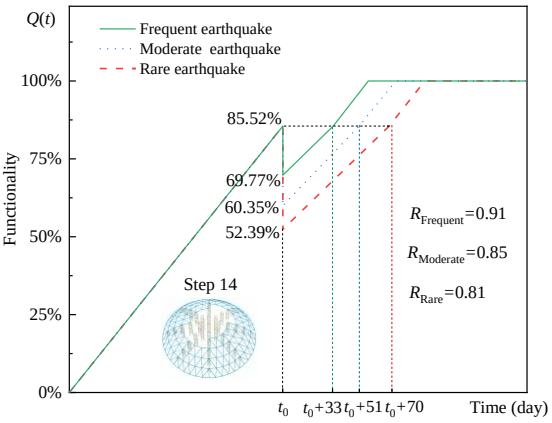


**Fig. 16** Seismic resilience of different earthquake hazards at construction step 14

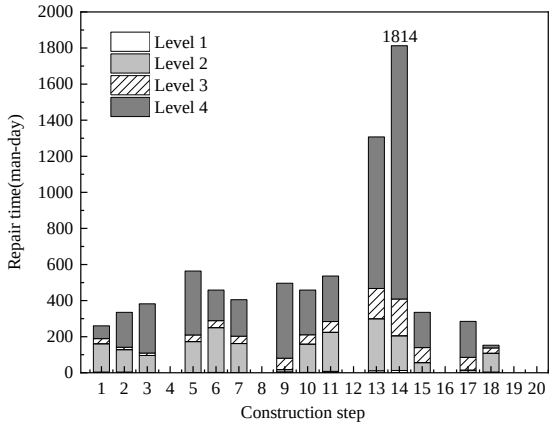


(a) Value of repair time

## 6. Summary and conclusions

By improving the curve of recovery functionality, the framework for seismic resilience assessment of a single-layer reticulated dome during construction was established in this study. The hysteresis analysis of the circular steel pipe under the combined action of bending moment and axial force was conducted by numerical simulation, and the damage state criterion of two failure modes was presented. Based on the advanced computational formulas of the repair time and recovery functionality considering different construction periods, the elastoplastic time-history analysis of an incomplete single-layer reticulated dome was carried out, and the seismic resilience during construction was assessed by using the Kiewitt-8 dome as an example. The main conclusions are as follows:

(1) There are two failure modes of the single-layer reticulated dome under seismic action: the bending failure mode caused by the bending moment and the axial failure mode caused by the axial force. Because members in single-layer reticulated domes often suffer from combined greater bending and greater axial force, the index of circular steel pipes at different damaged state levels obtained by the hysteretic curve and the skeleton curve is lower than the index in the existing Chinese standard. The damage state level of each member in the dome should be determined by the most unfavorable index calculated in the $M$-$\theta$ and $F$-$\Delta$ damage state criteria.

(2) The seismic bearing capacity of the complete single-layer reticulated dome is larger than that of the incomplete dome, and the seismic bearing capacity varies greatly under different construction periods. The number of damaged members and the percentage of member damage state levels are significantly influenced by the different construction stages. The construction models of the whole process must be established to find the most unfavorable construction state under seismic action.

(3) The repair time and the seismic resilience value of the incomplete dome also vary greatly under different construction periods. The repair time is related to the number of damaged members and the damage state levels of each damaged member. The repair time is longer if the number of damaged members is greater and the state level of the damaged member is higher. The seismic resilience of incomplete domes under earthquakes is smaller, and the

functionality of the dome under construction will decrease. Special measures should be taken to control the seismic safety of the most unfavorable construction periods by seismic resilience assessment.

## Acknowledgements

The authors acknowledge the financial support of the Hainan Provincial Natural Science Foundation of China (Grant No. 520QN232).

## References

[1] Fan F., Zhi X.D. and Shen S.Z., "Failure mechanism of large span reticulated shells subjected to severe earthquakes", Journal of Building structures, 31(6), 153-159, 2010. (in Chinese)
[2] Zhi X.D., Fan F. and Shen S.Z., "Failure and damage of single-layer reticulated cylindrical shells under earthquakes", China Civil Engineering Journal, 40(8), 29-34, 2007.(in Chinese)
[3] Nie G.B., Xie K., Zhi X.D. and Dai J.W., "Performance-based seismic design of reticulated shells", China Civil Engineering Journal, 51(S1), 8-12+19, 2018. (in Chinese)
[4] Liu X.W. and Guo Y.L., "State Nonlinear Finite Element Method for Construction Mechanics Analysis of Steel Structures", Engineering Mechanics, 25(10), 161-169, 2008. (in Chinese)
[5] Tian L.M., Hao J.P., Chen T., Zheng J. and Wang Y., "Simulation analysis on erection procedure of main stadium for the Universiade Sports Centre", Journal of Building structures, 32(05), 70-77, 2011. (in Chinese)
[6] Li Y.Y., Wang W. and Cao P.Z., "Comparison on Construction Schemes of the steel Shell in the Variety Hall of Jiangsu Grand Theater", Progress in Steel Building Structures, 20(01), 106-112, 2018. (in Chinese)
[7] Bruneau M, Chang S E, and Eguchi R T, "A framework to quantitatively assess and enhance the seismic resilience of communities", Earthquake Spectra, 19(4), 733-752, 2003.
[8] Vásquez A, Rivera F and De la Llera J, "Healthcare network's response and resilience in Iquique after the 2014 Pisagua earthquake", 16th World Conference on Earthquake Engineering, Paper No. 3639, 2017.
[9] Favier P, Rivera F and Poulos A, "Impact on chilean hospitals following the 2015 Illapel earthquake", 16th World Conference on Earthquake Engineering, Paper No. 4415, 2017.
[10] Domaneschi M, Martinelli L and Cimellaro G P, "Immediate seismic resilience of a controlled cable-stayed bridge", 16th World Conference on Earthquake Engineering, Paper No. 482, 2017.
[11] Biondini F, Capacci L and Titi A., "Life-cycle resilience of deteriorating bridge networks under earthquake scenarios", 16th World Conference on Earthquake Engineering, Paper No. 939, 2017.
[12] Dong Y and Frangopol D M., "Probabilistic assessment of an interdependent healthcare-bridge network system under seismic hazard", Structure and Infrastructure Engineering, 13(1), 160-170, 2017.
[13] Pang Y, Wei K and Yuan W., "Life-cycle seismic resilience assessment of highway bridges with fiber-reinforced concrete piers in the corrosive environment", Engineering Structures, 222:111120, 2020.
[14] Seismic performance assessment of buildings: Volume 1 - Methodology., Federal Emergency Management Agency, Washington D C, U.S., 2012.
[15] REDi rating system: resilience-based earthquake design initiative for the next generation of buildings., Arup Group, London, UK, 2013.
[16] Rating building performance in natural disasters., U.S. Resiliency Council, U.S., 2021.
[17] Code for seismic resilience assessment of buildings: GB/T 38591—2020., Standards Press of China, Beijing, China, 2020. (in Chinese)
[18] Lu X., "Seismic resilience evaluation of a reinforced concrete frame core tube structure", Journal of Building structures, 42(05), 55-63, 2021. (in Chinese)
[19] Fang D.P., Li Q.W. and Li N., "An evaluation system for community seismic resilience and its application in a typical community", Engineering Mechanics, 37(10), 28-44, 2020. (in Chinese)
[20] Fan S.G., Shu G.P., Lu Z.T. and Meng X.D., "Strengthening and Renovation Design of The Space Grid Structure After Fires", Industrial Construction, 32(10), 69-71+68, 2002. (in Chinese)
[21] Ren J.Y., Pan P., Wang T., Zhou Y., Wang H.S., Shan M.Y., "Interpretation of GB / T 38591—2020 'Standard for seismic resilience assessment of buildings'", Journal of Building Structures, 42(1), 48-56, 2021. (in Chinese)
[22] Xiao Y., Zhou Y., Wu H., Pan P. and Wang T., "Comparative study on GB / T 38591—2020 'Standard for seismic resilience assessment of buildings' and relevant international standards", Journal of Building Structures, 42(7), 194-202, 2021. (in Chinese)
[23] Cimellaro G P, Reinhorn A M and Bruneau M, "Framework for analytical quantification of disaster resilience", Engineering Structures, 32(11), 3639-3649, 2010.
[24] Code for seismic design of buildings: GB 50011—2016., China Architecture & Building Press, Beijing, China, 2016. (in Chinese)